Proximity-induced superconductivity in ferromagnetic Gd layers on Nb from a first-principles LDA + U study

Kyungwha Park [1,*] László Oroszlany,[2,3,†] László Szunyogh [4,5,‡] and Balázs Ujfalussy [3,§]

[1]*Department of Physics, Virginia Tech, Blacksburg, Virginia 24061, USA*

[2]*Department of Physics of Complex Systems, Eötvös University, Pázmány Péter sétány 1/A, H-1117 Budapest, Hungary*

[3]*Wigner Research Centre for Physics, Institute for Solid State Physics and Optics, H-1525 Budapest, Hungary*

[4]*Department of Theoretical Physics, Institute of Physics, Budapest University of Technology and Economics, Műegyetem rkp. 3., HU-1111 Budapest, Hungary*

[5]*BME Condensed Matter Research Group, Budapest University of Technology and Economics, Műegyetem rkp. 3., HU-1111 Budapest, Hungary*

(Received 6 August 2024; revised 11 October 2024; accepted 30 October 2024; published 14 November 2024)

We implement the on-site Coulomb repulsion U and exchange coupling J within the local density approximation (LDA) into the recently developed Dirac-Bogoliubov–de Gennes (DBdG) solver [G. Csire *et al.*, Phys. Rev. B **97**, 024514 (2018)] for superconducting heterostructures, by using the screened Korringa-Kohn-Rostoker (SKKR) Green's function method. We apply this implementation to ferromagnetic (FM) Gd layers on a superconducting Nb substrate, where the U and J terms are considered only for the $4f$ orbitals of the Gd layers, and investigate the proximity-induced superconducting properties of the Gd layers by using the implemented DBdG + U solver. Our first-principles calculations reveal that with the U and J terms, the density of states at the Fermi level has small contributions from $4f$ orbitals, while without the U and J terms, the contribution of the $4f$ orbitals somewhat increases. For the calculated quasiparticle density of states (DOS), with the U and J terms, there are several secondary satellite gaps, plateau-like regions, and central small V-shaped in-gap states within the bulk superconducting Nb gap, while without the U and J terms, the central V-shaped in-gap states appear within a much wider energy window. The in-gap states are identified to the Yu-Shiba-Rusinov states arising from the individual Gd layers with large magnetic moments rather than due to small magnetization induced in the Nb layers. We find that the normal-state DOS of the FM overlayers at the Fermi level is as important as the magnetic moment of the FM overlayers to the quasiparticle DOS. We also compute the superconducting order parameter as a function of the vertical z coordinate for 10 Gd layers on a Nb substrate. The order parameter abruptly decreases in the proximity to the interface and it oscillates as a function of the z coordinate in the Gd layers. This feature of quasiparticle DOS is qualitatively consistent with the previous studies. The implemented DBdG + U solver can be used to perform first-principles studies of other strongly correlated superconducting heterostructures as well as bulk superconductors.

DOI: 10.1103/PhysRevB.110.174510

I. INTRODUCTION

When FM metallic layers are overlaid on superconducting (SC) substrates, the Cooper pairs in the SC substrates penetrate the FM side, resulting in proximity-induced superconductivity in the FM layers. The magnetization of the FM layers induces an exchange field to the Cooper pairs in the FM side, which results in a spatially varying phase in the wave functions of the Cooper pairs or the SC order parameter [1]. As a result, the SC critical temperature oscillates with the thickness of FM layers.

One of the first experiments on FM-SC heterostructures was performed on Gd metallic layers on Nb substrates [2], where the SC critical temperature was observed to oscillate with the number of Gd layers. Similar oscillations were observed for Nb/Gd/Nb trilayers [3] and Nb/Au/Fe trilayers [4]. An experiment on Al/PdNi/Nb tunnel junctions revealed that the differential conductance was reversed as the thickness of PdNi layers increased, which indicated a change of the SC order parameter phase by π (Ref. [5]). Similar phenomena to this was also observed for Nb overlayers on CoFe layers [6].

The majority of the theoretical efforts in FM-SC heterostructures were made by solving either the Usadel equations for the Green's functions in the dirty limit [1,7–13] or the Bogoliubov–de Gennes (BdG) equations in the ballistic limit [14–16]. In these efforts, spin-orbit coupling (SOC) was often neglected except for Ref. [1], and interface effects might not be fully described by the introduced parameters. Recently, Csire *et al.* [17] developed a first-principles-based approach for SC heterostructures by solving the fully relativistic Dirac-Bogoliubov–de Gennes (DBdG) equations within

*Contact author: kyungwha@vt.edu
†Contact author: laszlo.oroszlany@ttk.elte.hu
‡Contact author: szunyogh.laszlo@ttk.bme.hu
§Contact author: ujfalussy.balazs@wigner.hu

the multiple scattering Green's function method [i.e., the screened Korringa-Kohn-Rostoker (SKKR) method]. In this approach, the band structures of FM (or non-SC) layers and SC substrates based on density-functional theory (DFT) were included in the SC state in the presence of SOC as well as scalar relativistic terms. When this approach was applied to Nb/Au/Fe trilayers, Csire *et al.* [17] showed oscillations of the SC order parameter, which was in good agreement with the experimental data reported by Ref. [4].

To apply the first-principles approach to the Gd atomic layers on Nb in the SC state, we need to address strong electron correlation in the Gd layers because the exchange splitting of the Gd layers is greatly affected by electron correlation and it also determines the periodicity of oscillations of the SC order parameter [11,13,14]. Anisimov *et al.* [18] showed that the exchange-field splitting value of bulk hcp Gd metal agreed with experimental data when on-site Coulomb repulsion U term and exchange term J were considered for $4f$ orbitals within DFT calculations. In this work, we implement the U and J terms into the DBdG solver within the SKKR Green's function method, following the implementation given by Refs. [18,19] in the normal state. Using our new implementation, we investigate the properties of the proximity-induced superconductivity for several Gd layers on Nb. Our implementation can be applied to some bulk strongly correlated superconductors and other SC heterostructures which require a good description of strong electron correlation.

In Sec. II we describe our computational methods and FM-SC heterostructures. In Sec. III we present the effect of the U and J terms on the exchange-field splitting of the systems of interest in the normal state. In Sec. IV we show the effect of the U and J terms on the quasiparticle density of states (DOS) as a function of FM layers and SC layers, the importance of coupling strength on the quasiparticle DOS, and layer-dependent SC order parameter. In Sec. V we make a conclusion.

II. COMPUTATIONAL DETAILS

A. Methods

The DBdG solver was developed by the authors of Ref. [17] within the SKKR method. The DBdG Hamiltonian [17] can be written as

$$\mathcal{H}_{\mathrm{DBdG}} = \begin{pmatrix} \mathcal{H}_{\mathrm{D}} & \Delta_{\mathrm{eff}}(r)\boldsymbol{\eta} \\ \Delta^*_{\mathrm{eff}}(r)\boldsymbol{\eta}^T & -\mathcal{H}^*_{\mathrm{D}} \end{pmatrix}, \tag{1}$$

where $\boldsymbol{\eta}$ is the time-reversal symmetry matrix [20]. Here Δ_{eff} is an effective pairing potential which is assumed to be $\lambda\chi(r)$, where λ is a semi-phenomenological electron-phonon coupling constant. Assuming a contact pairing potential, the relativistic order parameter $\chi(r)$ is defined to be $\langle\Psi(r)^T\boldsymbol{\eta}\Psi(r)\rangle$, where $\Psi(r)$ denotes four-component Dirac spinor field operator. The Dirac Hamiltonian $\mathcal{H}_{\mathrm{D}}$ in Rydberg units is given by

$$\mathcal{H}_{\mathrm{D}} = c\boldsymbol{\alpha}\mathbf{p} + (\boldsymbol{\beta} - \mathbb{I}_4)m_e c^2 + (V_{\mathrm{eff}}(\mathrm{r}) - E_{\mathrm{F}})\mathbb{I}_4 + \boldsymbol{\Sigma}\vec{B}_{\mathrm{eff}}(\mathrm{r}), \tag{2}$$

where

$$\boldsymbol{\alpha} = \begin{pmatrix} 0 & \boldsymbol{\sigma} \\ \boldsymbol{\sigma} & 0 \end{pmatrix}, \quad \boldsymbol{\beta} = \begin{pmatrix} \mathbb{I}_2 & 0 \\ 0 & -\mathbb{I}_2 \end{pmatrix}, \quad \boldsymbol{\Sigma} = \begin{pmatrix} \boldsymbol{\sigma} & 0 \\ 0 & \boldsymbol{\sigma} \end{pmatrix},$$
$$\mathbb{I}_4 = \begin{pmatrix} \mathbb{I}_2 & 0 \\ 0 & \mathbb{I}_2 \end{pmatrix}, \tag{3}$$

and $\boldsymbol{\sigma}$ are the Pauli matrices and $\mathbb{I}_2$ is a 2×2 identity matrix. Here $\mathbf{p}$ and E_{F} are the momentum operator and the Fermi level, respectively. c and m_e are the speed of light and electron mass, respectively. $V_{\mathrm{eff}}(\mathrm{r})$ denotes the effective electrostatic potential and $\vec{B}_{\mathrm{eff}}(r)$ represents the effective exchange field. Within the SKKR multiple scattering theory, the relativistic Green's function can be written as

$$G^{ab}(z,\vec{r},\vec{r}) = \sum_n \frac{\Psi^a_n(z,\vec{r})\left[\Phi^b_n(z,\vec{r})\right]^\dagger}{z - E_n(z)}, \tag{4}$$

where $z = \epsilon + i\delta$ and $E_n(z)$ is the energy of the orbital degrees of freedom n. Here Ψ^a_n and Φ^b_n are the right-hand-side and left-hand-side solutions of the DBdG equations, respectively. The indices a and b run for electron and hole components.

The LDA + U method [18] (LDA: local density approximation) was implemented in the normal state by Ref. [19] within the SKKR method, and magnetic properties of bulk Gd in the FM and paramagnetic state were studied. With $U = 6.7$ eV and $J = 0.7$ eV [18] for $4f$ orbitals, the authors of Ref. [19] showed that the calculated exchange-field splitting of bulk Gd metal was about 11 eV, which is in good agreement with experimental data [21,22].

We implement the LDA + U method [18] into the existing DBdG solver [17] within the SKKR Green's function method, following the procedures in Ref. [19]. The effects of U and J enter into the relativistic Hartree-Fock potential $V_{QQ'}$

$$V_{QQ'} = \sum_{\sigma,\sigma'} C\left(l, j, \frac{1}{2}; \mu-\sigma, \mu, \sigma\right) V^{\sigma,\sigma'}_{\mu-\sigma,\mu'-\sigma'} \times C\left(l, j', \frac{1}{2}; \mu'-\sigma', \mu', \sigma'\right), \tag{5}$$

$$V^{\sigma,\sigma'}_{\mu-\sigma,\mu'-\sigma'} = \delta_{\mu-\sigma,\mu'-\sigma'}\delta_{\sigma,\sigma'}(U-J)\left(\frac{1}{2} - \frac{n_\sigma}{2l+1}\right), \tag{6}$$

where $Q = \kappa, \mu$ and $Q' = \kappa', \mu'$. Here κ, κ', μ, and μ' are relativistic angular momentum quantum numbers [23]. l and j are orbital and total angular momentum quantum numbers, respectively, and n_σ is the occupancy of spin σ. $C(l, j, \frac{1}{2}; \mu-\sigma, \mu, \sigma)$ and $C(l, j', \frac{1}{2}; \mu'-\sigma', \mu', \sigma')$ are the Clebsch-Gordan coefficients. The potential $V_{QQ'}$ is added to the diagonal elements $u^{++}_{QQ'}(r)$ of the large components of the electron and hole part of the right-hand side matrices of the radial right-hand side and left-hand side DBdG equations (Eqs. (15) and (22) in Ref. [17]). More specifically, Eq. (16) in Ref. [17] is modified into

$$u^{++}_{QQ'}(r) = V(r) + \sum_{i=x,y,z} \langle\tilde{\chi}_Q|\sigma_i B^i_{\mathrm{eff}}(r)|\tilde{\chi}_{Q'}\rangle + V_{QQ'}, \tag{7}$$

where $V(r)$ is an external potential, $\tilde{\chi}_{Q,Q'}$ are spin spherical harmonics, and B^i_{eff} is an ith component of the external exchange field. Other than this modification, the rest of the

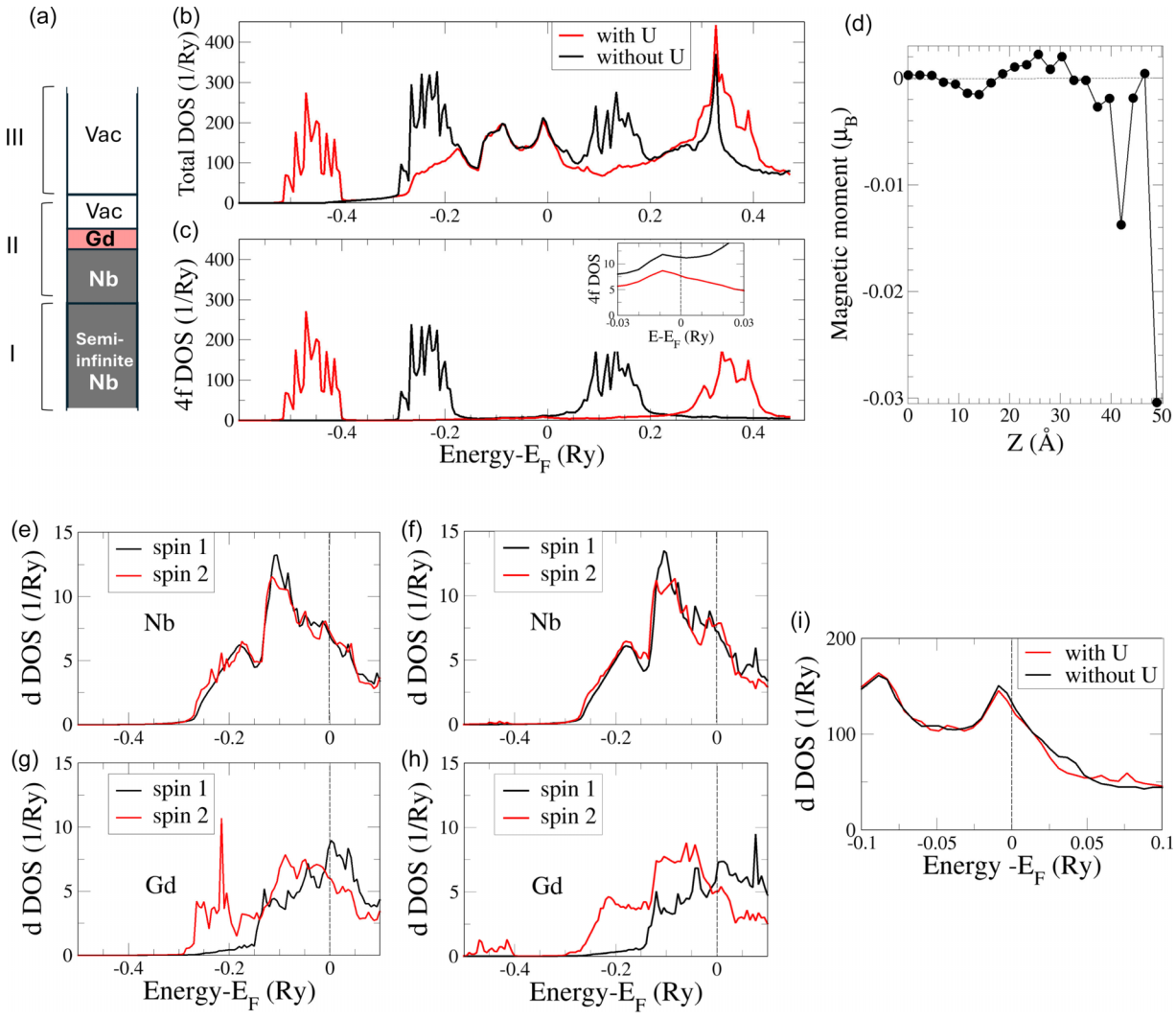

FIG. 1. (a) Schematic diagram of Gd layers on a Nb(110) substrate where the middle interface region consists of several Gd layers and some Nb layers as well as several vacuum layers. (b),(c) Normal-state total DOS and DOS projected onto $4f$ orbitals with and without U and J for 2 Gd layers on Nb(110) where 6 Nb layers are included in the interface region. The inset of (c) shows zoom-in of (c) near the Fermi level. (d) Magnetic moments induced in the interface Nb layers for 2 Gd layers overlaid on 22 interface Nb layers in the presence of U and J. (e),(f) The DOS projected onto d orbitals of the topmost Nb layer without and with U and J. (g),(h) The DOS projected onto d orbitals of the interface Gd layer without and with U and J. (i) The DOS projected onto d orbitals of all atoms with and without U and J. For (e)–(i), 2 Gd layers overlaid on six interface Nb layers are considered.

procedures are the same as in Refs. [17,19]. This implementation is referred to as the DBdG + U solver.

First, we construct a heterostructure of semi-infinite Nb, some Gd layers, and semi-infinite vacuum by using the SKKR method. Potentials representing several Nb layers and vacuum layers are allowed to be relaxed along with the Gd potentials during the self-consistent field cycles. This region consisting of the relaxed Nb and vacuum layers with Gd layers is referred to as the interface region. The potentials are relaxed with an orbital angular momentum cutoff of $l_{\max} = 3$ and 916 k points in the two-dimensional irreducible Brillouin zone [equivalent to 3664 k points in the full two-dimensional (2D) BZ] by using the SKKR method within Kohn-Sham-Dirac density functional theory (DFT) in the atomic sphere approximation, where $U = 6.7\,\text{eV}$ and $J = 0.7\,\text{eV}$ are included for the $4f$ orbitals in Gd. We use the radii for the Nb and Gd atoms 1.6250 and 1.6899 Å, respectively. For the interface Nb atom, we use the radius of 1.6581 Å. For all of the calculations, we use the Vosko-Wilk-Nusair local spin density approximation [24]. Now the normal-state converged potentials are fed into the DBdG + U solver in the SC state. The number of k points in the two-dimensional irreducible Brillouin zone in the SC state is the same as in the normal state. The pairing potential of the bulk Nb is set to be same as the experimental SC gap, Δ_{bulkNb}, 1.52 meV (=0.112 mRy) [25]. The pairing potential of the Nb layers in the interface region is set to be same as that of the bulk Nb, while the pairing potential of the Gd layers and the vacuum layers are set to be zero. To compute the SC order parameter, one self-consistent field run is completed in the SC state. Note that the SC pairing potential, the SC order parameter, and the SC gap, are *not* equivalent quantities for inhomogeneous superconductors, although they are equivalent for homogeneous superconductors. DOS in the normal state is computed using a broadening (i.e., the imaginary part of

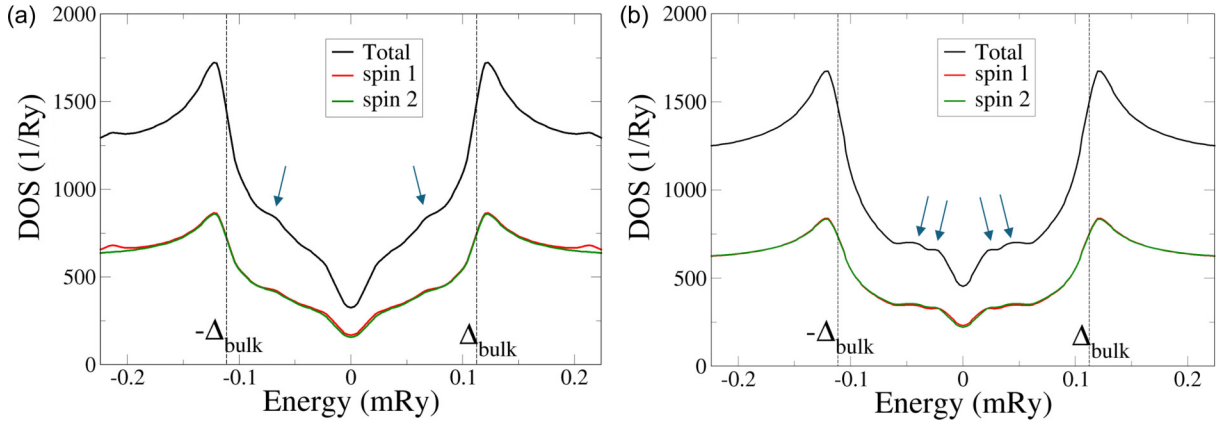

FIG. 2. SC-state DOS (a) without U and J and (b) with U and J for 2 Gd layers on Nb(110) where 22 Nb layers are included in the interface region. Spin-up and spin-down DOS are also separately shown. Small arrows in (a) and (b) indicate secondary small peaks.

the energy) of 0.5 mRy, while quasiparticle DOS in the SC state is calculated using a broadening of 10 μRy.

B. Systems of interest

In experimental samples of Gd(001)/Nb(110) bilayers [2,26], a large commensurate supercell is formed due to different crystal structures between Gd and Nb. However, one cannot simulate such a large supercell within the standard SKKR Green's function method due to the high computational cost. Instead, we consider a single Gd or Nb atom per layer. The heterostructure of interest consists of several Gd layers stacked on a semi-infinite Nb(110) substrate with a semi-infinite vacuum. Note that there are some relaxed Nb layers between the Gd layers and the semi-infinite Nb, as mentioned earlier. The in-plane lattice constants are set to be a_{Nb} (=3.3004 Å) and $\sqrt{2}a_{\mathrm{Nb}}$ (=4.6675 Å) along the [001] and [$\bar{1}$10] directions, respectively, following the experimental values of bulk Nb [27]. The vertical interlayer distance of the Nb layers is $a_{\mathrm{Nb}}/\sqrt{2}$ (=2.3370 Å), while the vertical distance of the Gd layers is set to be $c_{\mathrm{Gd}}(a_{\mathrm{Nb}}/a_{\mathrm{Gd}})/2$ (=2.6244 Å) considering the experimental bulk Gd lattice constants [28]. The vertical distance between the topmost Nb and the bottommost Gd atomic layers is set to be the same as that between neighboring Gd layers. Figure 1(a) shows our simulated heterostructure consisting of semi-infinite Nb (region I), interface region (region II comprising some Nb layers, Gd layers, and vacuum layers), and a semi-infinite vacuum (region III).

III. NORMAL-STATE PROPERTIES

In the normal state, our SKKR calculation on bulk fcc Gd metal suggests that the exchange splitting is 0.38 Ry (=5.17 eV) without U and J, while it increases to 0.76 Ry (=10.34 eV) when $U = 6.7$ eV and $J = 0.7$ eV are considered for $4f$ orbitals. Figures 1(b) and 1(c) show calculated total DOS and Gd $4f$ DOS in the normal state for the two Gd layers on Nb(110) with and without U and J, respectively, when six Nb layers are included in the interface region. Without U and J, the exchange splittings for the total DOS and Gd $4f$ DOS is 5.2 eV. With U and J, the exchange splitting greatly increases and becomes comparable to the splitting of bulk Gd metal, and the DOS at the Fermi level E_{F} slightly decreases [see the inset of Fig. 1(c)].

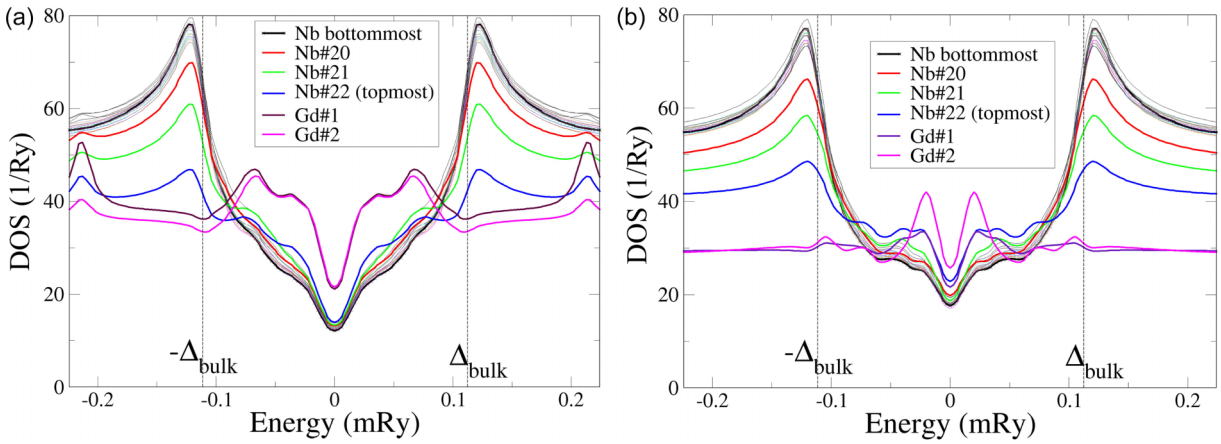

FIG. 3. Layer-dependent SC-state DOS of the interface region for two Gd layers on Nb(110) when 22 Nb layers are included in the interface (a) without U and J and (b) with U and J. Nb#1 (Nb#22) denotes the bottommost (topmost) Nb layer.

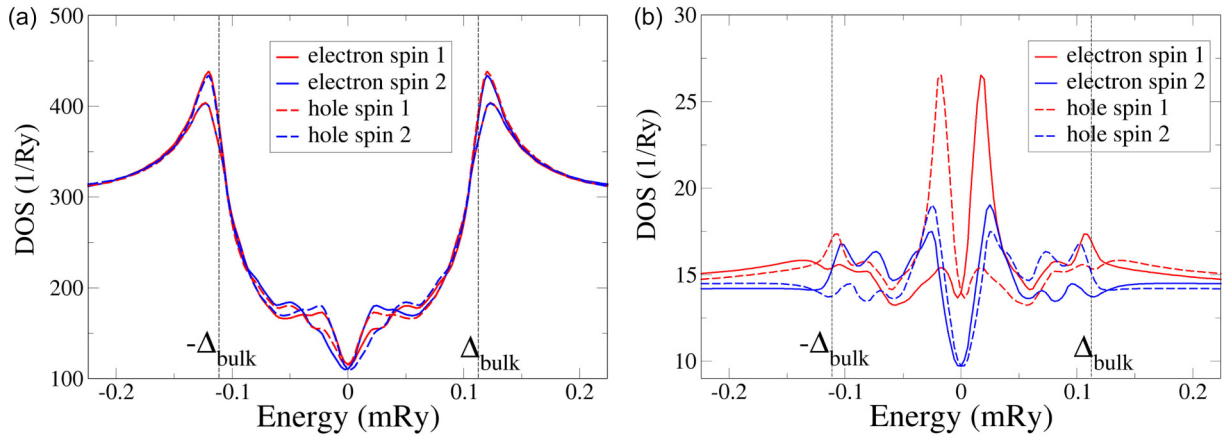

FIG. 4. Spin-resolved electron and hole components of (a) the total DOS in the interface and (b) the Gd layers for two Gd layers on Nb(110) when 22 Nb layers are included in the interface.

Table I lists our calculated magnetic moments of the two Gd layers on Nb(110) with and without U and J. With U and J the magnitude of the magnetic moments are calculated to be 8.0 and 8.1 μ_B within the Wigner-Seitz radius, which are close to what we expect for Gd with strongly localized $4f$ orbitals as well as a singly occupied $5d$ orbital. Without U and J the magnetic moments noticeably decrease due to much less localized $4f$ orbitals. We also calculate magnetic moments induced in the interface Nb layers. With U and J the magnitude of the maximum induced magnetic moment is found to be 0.03 μ_B at the topmost Nb layer, while without U and J the magnitude of the maximum moment is at most 0.01 μ_B at the topmost Nb layer. Figure 1(d) shows the magnetic moments in the Nb layers induced by the Gd layers when the two Gd layers are overlaid on 22 interface Nb layers with U and J. A very small induced moment is found even the bottommost Nb layer and it fluctuates as a function of the distance away from the interface.

It is interesting to observe the d-orbital contribution to the DOS and spin-polarization by computing the d-orbital DOS at the interface Gd layer and the topmost Nb layer for the two Gd layers overlaid on the six interface Nb layers. As seen in Figs. 1(e) to 1(h), for the Gd layer, the DOS clearly shows the spin-2 (spin-down) polarization, while for the Nb layer, the spin polarization is not apparent due to a small, induced spin polarization. With U and J, the d-orbital spin polarization from the Gd layer at the Fermi level is quite reduced compared to that without U and J [i.e., compare Figs. 1(g) to 1(h)]. For the Gd layer, the d-orbital contribution to the DOS and spin-polarization at the Fermi level is much higher than the f-orbital contribution. The d-orbital DOS from all of the atoms at the Fermi level with U and J is slightly lower than that without U and J, as shown in Fig. 1(i).

TABLE I. The Gd magnetic moments in μ_B (Bohr magneton) with and without U and J for two Gd layers overlaid on 22 Nb interface layers. The second Gd layer, Gd(2), is in contact with the vacuum layer.

Type	With U and J	Without U and J
m[Gd(1)](μ_B)	−8.0	−7.5
m[Gd(2)](μ_B)	−8.1	−7.7

IV. SUPERCONDUCTING PROPERTIES

A. Effect of U and J on DOS: 2 Gd layers on Nb

We calculate the quasiparticle DOS for two Gd layers on Nb(110) with 22 Nb layers in the interface region in the SC state. Without U and J, a sharp deep V-shaped DOS appears within the SC gap of bulk Nb [see Fig. 2(a)], and there are secondary small peaks near ±0.075 mRy within the SC gap. There are also the usual large peaks right above (below) Δ_{bulkNb} ($-\Delta_{\text{bulkNb}}$). With U and J, the overall shape of the DOS changes significantly [see Fig. 2(b)]. The DOS has quite flat regions with tiny peaks near ±0.025 and ±0.04 mRy within the SC gap, and there is a small shallow V-shaped in-gap states within the energy window of ±0.025 mRy. The features of the observed in-gap states quite differ from those in the case without U and J. The difference is attributed to more localized $4f$ orbitals as well as resultant changes in the $5d$ orbitals in the case with U and J. Note that at the Fermi level, the $4f$ and $5d$ orbital contributions are much less with U and J than those without U and J.

To understand better the origin of the in-gap states, we compute individual layer-dependent quasiparticle DOS in the SC state when two Gd layers are overlaid on 22 Nb layers in the interface region (see Fig. 3). The atomic layers in the interface region are labeled as Nb(1)-Nb(2)-...-Nb(20)-Nb(21)-Nb(22)-Gd(1)-Gd(2)-Vac(1)-Vac(2)-Vac(3)-Vac(4) starting from the bottommost Nb layer to the topmost vacuum layer. We first discuss the case with U and J. The bottom 19 Nb layers have DOS features similar to the bare Nb layers in the vicinity of bulk SC gap and beyond the SC gap region. For example, the heights of the DOS peaks of the Nb layers near $\pm\Delta_{\text{bulk}}$ are almost the same as those of the pristine Nb layers. However, significant in-gap states are found for all of these 19 Nb interface layers with a V shape within ±0.09 mRy. The fact that the in-gap states are formed on all Nb layers is consistent with the fact that the thickness of the interface Nb layers is too small compared to the SC coherence length of Nb (which is about several tens of nanometers). The height of the DOS peak near the bulk SC gap strongly decreases

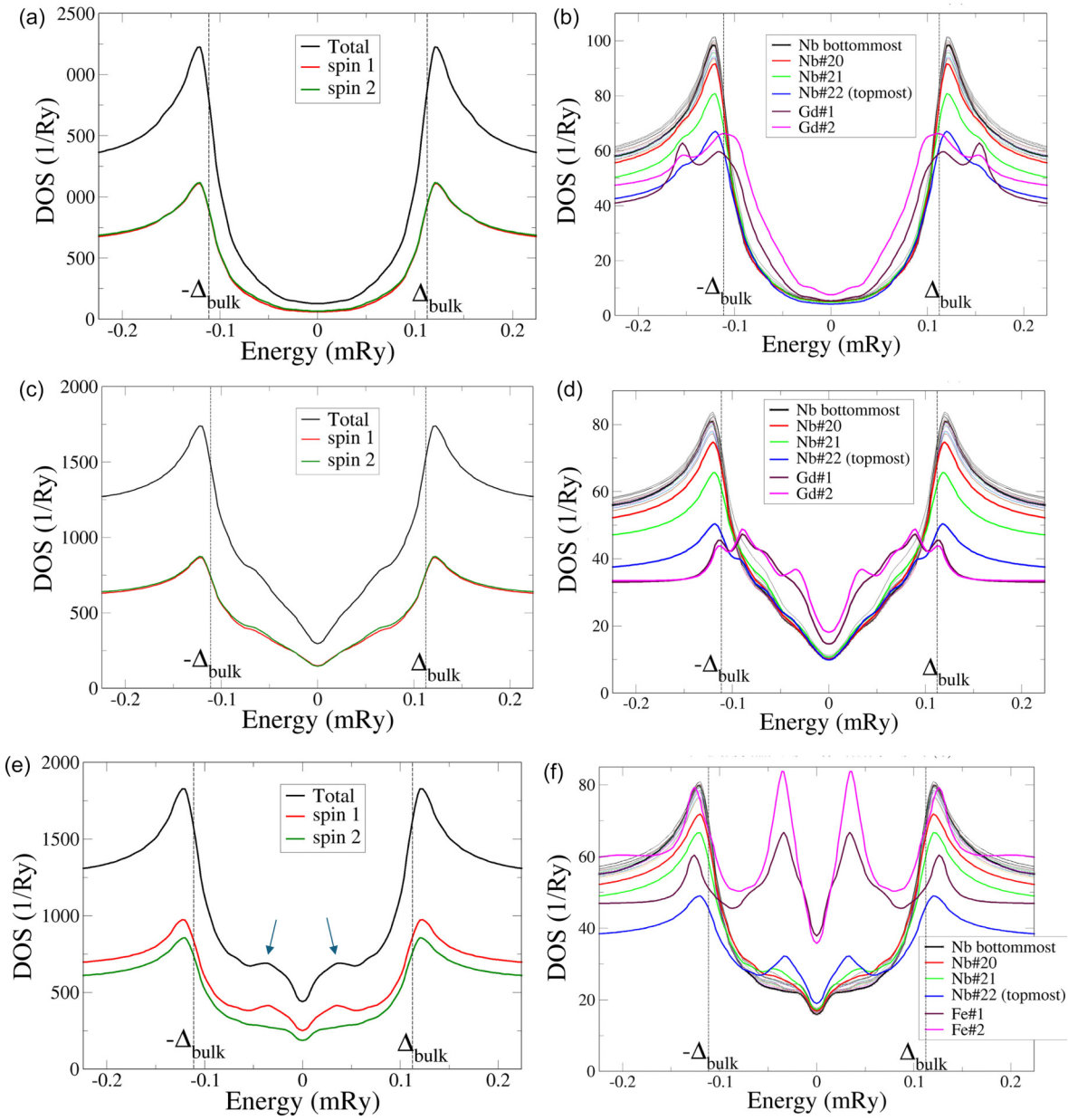

FIG. 5. SC-state DOS for 2 Gd layers on Nb with 22 interface Nb layers when the Gd exchange field is scaled by a factor of (a) 0.1 and (c) 0.375. (b),(d) Corresponding layer-dependent SC-state DOS for (a),(c), respectively. (e),(f) SC-state DOS and layer-dependent DOS for two Fe layers on Nb with 22 interface Nb layers. The magnetic moment of Fe is close to that of Gd whose the exchange field is scaled by 0.375.

for the Nb(20), Nb(21), and Nb(22) layers. Specifically, the in-gap states near the Fermi level increases noticeably for the Nb(20), Nb(21), and Nb(22) layers. For the Gd(1) and Gd(2) layers, the DOS is found to be flat outside the bulk SC gap and there are substantial V-shaped (or upside-down W-shaped) in-gap states near the Fermi level. Without U and J the overall features of individual layer-dependent DOS related to the total DOS are similar to those of the case with U and J. One prominent difference is that without U and J the Gd(1) and Gd(2) layers contribute noticeably more to the in-gap states than those with U and J. Additionally, without U and J the peaks near $\pm 2\Delta_{\text{bulk}}$ are induced by the two Gd layers. These differences seem to be consistent with the observation that the DOS at the Fermi level is somewhat reduced with U and J. Unless specified otherwise, we, henceforth, consider the case with U and J.

Regarding the origin of the in-gap states, the scanning tunneling microscopy (STM) experiments on FM $SrRuO_3$ metallic layers on underdoped cuprates [29] proposed that the observed V-shaped in-gap states might be attributed to magnetic moments induced in the cuprates by $SrRuO_3$. To investigate the origin of the in-gap states, we deliberately set the induced magnetic moments of the 22 interface Nb layers to be zero, and calculate the quasiparticle DOS. We find that there are still in-gap states very similar to those with the nonzero induced magnetic moments. We, therefore, interpret

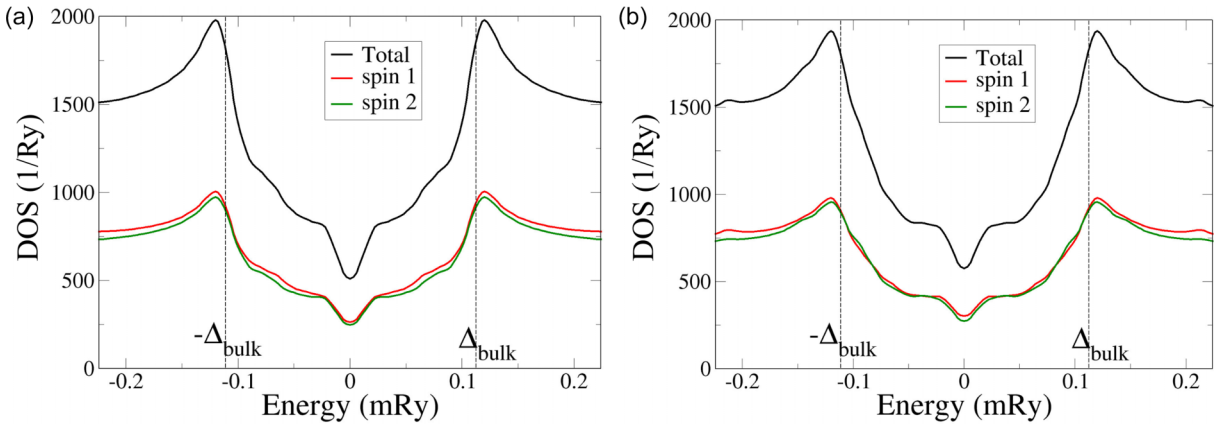

FIG. 6. SC-state DOS (a) for nine Gd layers on 23 Nb layers in the interface region and (b) for 10 Gd layers on 22 Nb layers in the interface region.

that the observed in-gap states in the Nb layers (Fig. 3) are not due to the induced magnetic moments, but a consequence of the Cooper pairs which are affected by the Gd exchange field in the Nb layers, i.e., Yu-Shiba-Rusinov (YSR) states [30–32]. Similar YSR states were observed for STM experiments on Mn layers on Nb [33].

B. Electron and hole components: Total and Gd DOS

We further analyze the quasiparticle DOS of 2 Gd layers on Nb by decomposing it into spin-1 and spin-2 electron and hole parts. Figure 4(a) shows spin-resolved electron and hole components of the total DOS for 2 Gd layers on Nb. The spin-1 (spin-2) electron component is similar to the spin-2 (spin-1) hole component, which is attributed to the SC nature of the Nb layers. The small difference between the spin-1 (spin-2) electron and the spin-2 (spin-1) hole components is more noticeable inside the SC gap. This is caused by the Gd layers, as shown in Fig. 4(b). For the Gd layers, similarities between the spin-1 (spin-2) electron component and the spin-2 (spin-1) hole component are much poorer than the Nb layers. The large electron-hole asymmetry in the Gd layers can be viewed as a signature of the YSR states.

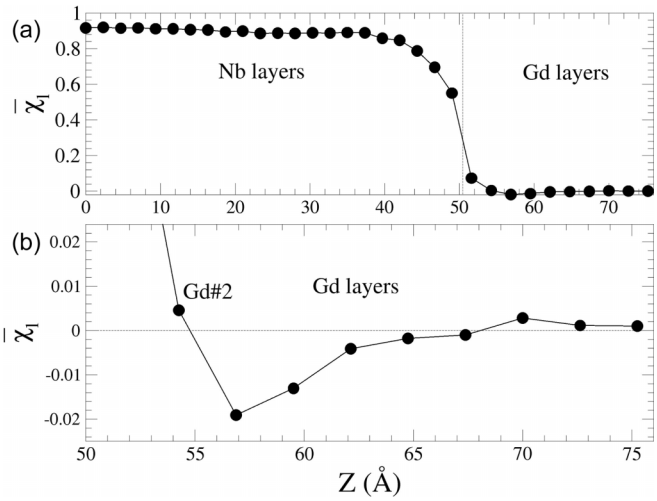

FIG. 7. (a) SC order parameter for the ten Gd layers on Nb(110) when 22 Nb layers are included in the interface region. (b) Zoom-in of (a) for ten Gd layers.

C. Effect of exchange field strength

We showed earlier that the exchange field or magnetic moment of the Gd layers induces the in-gap states. To further examine the effect of exchange field on SC-state DOS, we scale the Gd exchange field by factors of 0.1, 0.375, 0.5, and 0.75 for two Gd layers with 22 interface Nb layers, and compute corresponding quasiparticle DOS. Note that there is still a semi-infinite stack of Nb layers beneath the 22 Nb interface layers. For the factor of 0.1, the DOS has a U shape which is very similar to that of the pristine Nb case, and even the DOS of the Gd layers with the scaled exchange field also follows a U shape [Figs. 5(a) and 5(b)]. For the factor of 0.375, the DOS shows large V-shaped in-gap states, while it maintains a U shape at the edge of the bulk SC gap [Figs. 5(c) and 5(d)]. The DOS of the Gd layers is significantly different from that of the 22 interface Nb layers, but it overall follows the trend of the DOS of the 22 interface Nb layers within the SC gap. For a factor of 0.5, the features of the DOS look similar to those for the factor of 0.375. For the factor of 0.75, the DOS features resemble those for the factor of 1.0.

We now compare the SC-state DOS for the scaling factor of 0.375 with that for two Fe layers with 22 interface Nb layers [see Figs. 5(e) and 5(f)]. The magnetic moment of each Fe layer is about 3.0 μ_B which is about 0.375 of the magnetic moment of each Gd layer. The atomic coordinates of the Fe case are identical to those of the Gd case. In the Fe case, the DOS has overall very similar in-gap states and features to that of the Gd case for the scaling factor of 1. The DOS in the Fe case qualitatively differs from that for the scaling factor of 0.375, despite the same exchange fields in the two cases. Interestingly, in the Fe case, the spin-1 and spin-2 contributions are quite different from each other, and the small secondary peaks at ± 0.04 mRy are induced by the Fe layers. The Fe layers contribute to the total quasiparticle DOS much more than the Gd layers. Our result suggests that the exchange field alone does not fully capture the features of the quasiparticle DOS. We observe that the Fe case has

substantially higher normal-state DOS of the FM layers at the Fermi level than the Gd case, which results in a stronger coupling between the Fe overlayers and the Nb substrate than the coupling between the Gd layers and the Nb substrate. An importance of the normal-state DOS at the Fermi level on YSR states was emphasized in FM impurities on SC substrates [34].

D. Effect of Gd layer thickness

We investigate the effect of the thickness of Gd layers on the SC-state DOS. We consider two cases: (i) nine Gd layers on 23 interface Nb layers and (ii) ten Gd layers on 22 interface Nb layers. For the nine Gd layers on Nb [Fig. 6(a)], two secondary peaks appear near ± 0.025 and ± 0.08 mRy with the central V-shaped in-gap states within the SC gap. For the ten Gd layers on Nb [Fig. 6(b)], the central V-shaped in-gap states appear with plateaus nearby.

E. SC order parameter

We calculate the SC order parameter for each layer l, $\overline{\chi_l}$, by taking a ratio between the SC order parameter of the heterostructure and that of the bulk Nb as follows:

$$\overline{\chi_l} = \frac{\int_{\mathrm{WS}} dr \chi_l(r)}{\int_{\mathrm{WS}} dr \chi_{\mathrm{Nb,bulk}}(r)}, \tag{8}$$

where the integral runs over the atomic sphere of the Wigner-Seitz radius. Figure 7 shows the calculated SC order parameter for the 10 Gd layers on 22 interface Nb layers relative to that for bulk Nb. The order parameter of the bottommost interface Nb layer is about 92% of that of the bulk Nb. The calculated order parameter abruptly decreases in close proximity to the interface, and it oscillates within the Gd layers as a function of z coordinates (where the z axis is normal to the surface). The order parameter of the Gd layers becomes, at most, a few percents of that of the bulk Nb, and it even reverses its sign beyond the second Gd layer from the interface. Then it comes back to the small positive value at the eighth Gd layer from the interface. Qualitatively, these oscillations agree well with those in the SC order parameter discussed in the literature (Fig. 3 in Ref. [1]).

V. CONCLUSION

We studied the proximity-induced superconductivity for FM Gd layers on Nb(110) by implementing the LDA + U method [18,19] into the recently developed DBdG solver [17], within the SKKR Green's function formalism. When $U = 6.7$ eV and $J = 0.7$ eV are considered for Gd $4f$ orbitals, the contributions of $4f$ and $5d$ orbitals to the Fermi level are somewhat reduced compared to the case without U and J. Overall, the quasiparticle DOS of the Gd layers shows V-shaped in-gap states about the Fermi level with several secondary gaps within the bulk Nb SC gap. Such in-gap states are attributed to YSR states arising from the exchange field of the Gd layers. In addition to the exchange field of Gd layers, we found that the normal-state DOS of the FM overlayers at the Fermi level plays an important role in the features of the in-gap states. For the ten Gd layers on Nb, we calculated the SC order parameter obtained from one self-consistent run, finding an oscillating SC order parameter in the Gd layers. This feature qualitatively agrees with model Hamiltonian studies [1,13] and experimental data [2]. Our implementation can be applied to other SC heterostructures where U and J terms are required for a good description of the electronic structure.

ACKNOWLEDGMENTS

K.P. gratefully acknowledges financial support by the Fulbright U.S. Scholar Program, which is sponsored by the U.S. Department of State and the Hungarian-American Fulbright Commission for Educational Exchange in Hungary. The computational support was provided by the Virginia Tech Advanced Research Computing (ARC) and through allocation DMR060009N from the Advanced Cyberinfrastructure Coordination Ecosystem: Services and Support (ACCESS) program [35], which is supported by National Science Foundation Grants No. 2138259, No. 2138286, No. 2138307, No. 2137603, and No. 2138296. B.U. acknowledges financial support by the National Research, Development, and Innovation Office (NRDI Office) of Hungary under Projects No. K131938 and No. K142652. L.S. was supported by the NRDI Office of Hungary under Projects No. K131938 and No. K142179. Further funding was provided by the Ministry of Culture and Innovation and the National Research, Development and Innovation Office under Grant No. TKP2021-NVA-02.

[1] E. A. Demler, G. B. Arnold, and M. R. Beasley, Superconducting proximity effects in magnetic metals, Phys. Rev. B **55**, 15174 (1997).

[2] J. S. Jiang, D. Davidović, D. H. Reich, and C. L. Chien, Oscillatory superconducting transition temperature in Nb/Gd multilayers, Phys. Rev. Lett. **74**, 314 (1995).

[3] Y. N. Khaydukov, A. S. Vasenko, E. A. Kravtsov, V. V. Progliado, V. D. Zhaketov, A. Csik, Y. V. Nikitenko, A. V. Petrenko, T. Keller, A. A. Golubov, M. Y. Kupriyanov, V. V. Ustinov, V. L. Aksenov, and B. Keimer, Magnetic and superconducting phase diagram of Nb/Gd/Nb trilayers, Phys. Rev. B **97**, 144511 (2018).

[4] H. Yamazaki, N. Shannon, and H. Takagi, Interplay between superconductivity and ferromagnetism in epitaxial Nb(110)/Au(111)/Fe(110) trilayers, Phys. Rev. B **73**, 094507 (2006).

[5] T. Kontos, M. Aprili, J. Lesueur, and X. Grison, Inhomogeneous superconductivity induced in a ferromagnet by proximity effect, Phys. Rev. Lett. **86**, 304 (2001).

[6] S. Reymond, P. SanGiorgio, M. R. Beasley, J. Kim, T. Kim, and K. Char, Tunneling density of states as a function of thickness in superconductor/strong ferromagnet bilayers, Phys. Rev. B **73**, 054505 (2006).

[7] A. I. Buzdin, L. N. Bulaevskii, and S. V. Panyukov, Critical-current oscillations as a function of the exchange field and thickness of the ferromagnetic metal (F) in an S-F-S Josephson junction, JETP Lett. **35**, 178 (1982).

[8] A. I. Buzdin and M. Y. Kupriyanov, Transition temperature of a superconductor-ferromagnet superlattice, JETP Lett. **52**, 487 (1990).

[9] A. I. Buzdin and M. Y. Kupriyanov, Josephson junction with a ferromagnetic layer, JETP Lett. **53**, 321 (1991).

[10] Z. Radović, L. Dobrosavljević-Grujić, A. I. Buzdin, and J. R. Clem, Upper critical fields of superconductor-ferromagnet multilayers, Phys. Rev. B **38**, 2388 (1988).

[11] Z. Radović, M. Ledvij, L. Dobrosavljević-Grujić, A. I. Buzdin, and J. R. Clem, Transition temperatures of superconductor-ferromagnet superlattices, Phys. Rev. B **44**, 759 (1991).

[12] A. Buzdin, Density of states oscillations in a ferromagnetic metal in contact with a superconductor, Phys. Rev. B **62**, 11377 (2000).

[13] A. I. Buzdin, Proximity effects in superconductor-ferromagnet heterostructures, Rev. Mod. Phys. **77**, 935 (2005).

[14] K. Halterman and O. T. Valls, Proximity effects at ferromagnet-superconductor interfaces, Phys. Rev. B **65**, 014509 (2001).

[15] K. Halterman and O. T. Valls, Proximity effects and characteristic lengths in ferromagnet-superconductor structures, Phys. Rev. B **66**, 224516 (2002).

[16] K. Halterman and O. T. Valls, Energy gap of ferromagnet–superconductor bilayers, Physica C: Superconductivity **397**, 151 (2003).

[17] G. Csire, A. Deák, B. Nyári, H. Ebert, J. F. Annett, and B. Újfalussy, Relativistic spin-polarized KKR theory for superconducting heterostructures: Oscillating order parameter in the Au layer of Nb/Au/Fe trilayers, Phys. Rev. B **97**, 024514 (2018).

[18] V. I. Anisimov, F. Aryasetiawan, and A. I. Lichtenstein, First-principles calculations of the electronic structure and spectra of strongly correlated systems: The LDA+*U* method, J. Phys.: Condens. Matter **9**, 767 (1997).

[19] L. Oroszlány, A. Deák, E. Simon, S. Khmelevskyi, and L. Szunyogh, Magnetism of gadolinium: A first-principles perspective, Phys. Rev. Lett. **115**, 096402 (2015).

[20] K. Capelle and E. K. U. Gross, Relativistic framework for microscopic theories of superconductivity. I. The Dirac equation for superconductors, Phys. Rev. B **59**, 7140 (1999).

[21] J. E. Ortega, F. J. Himpsel, D. Li, and P. A. Dowben, Initial and final state contributions of the core level shifts for Gd(0001), Solid State Commun. **91**, 807 (1994).

[22] S. Abdelouahed, N. Baadji, and M. Alouani, Electronic structure and x-ray magnetic circular dichroism of gadolinium beyond the local spin density approximation, Phys. Rev. B **75**, 094428 (2007).

[23] J. Zabloudil, R. Hammerling, L. Szunyogh, and P. Weinberger, *Electron Scattering in Solid Matter: A Theoretical and Computational Treatise*, 1st ed. (Springer, New York, 2005).

[24] S. H. Vosko, L. Wilk, and M. Nusair, Accurate spin-dependent electron liquid correlation energies for local spin density calculations: A critical analysis, Can. J. Phys. **58**, 1200 (1980).

[25] J. P. Carbotte, Properties of boson-exchange superconductors, Rev. Mod. Phys. **62**, 1027 (1990).

[26] J. Kwo, M. Hong, and S. Nakahara, Growth of rare earth single crystals by molecular beam epitaxy: The epitaxial relationship between hcp rare earth and bcc niobium, Appl. Phys. Lett. **49**, 319 (1986).

[27] M. E. Straumanis and S. Zyszczynski, Lattice parameters, thermal expansion coefficients and densities of Nb, and of solid solutions Nb–O and Nb–N–O and their defect structure, J. Appl. Crystallogr. **3**, 1 (1970).

[28] F. H. Spedding, A. H. Daane, and K. W. Herrmann, The crystal structures and lattice parameters of high-purity scandium, yttrium and the rare earth metals, Acta Crystallogr. **9**, 559 (1956).

[29] I. Asulin, O. Yuli, G. Koren, and O. Millo, Evidence for induced magnetization in superconductor-ferromagnet heterostructures: A scanning tunneling spectroscopy study, Phys. Rev. B **79**, 174524 (2009).

[30] L. Yu, Bound state in superconductors with paramagnetic impurities, Acta Phys. Sin. **21**, 75 (1965).

[31] H. Shiba, Classical spins in superconductors, Prog. Theor. Phys. **40**, 435 (1968).

[32] A. I. Rusinov, Superconductivity near a paramagnetic impurity, JETP Lett. (USSR) (Engl. Transl.) (United States) **9**, 85 (1969).

[33] R. Lo Conte, M. Bazarnik, K. Palotás, L. Rózsa, L. Szunyogh, A. Kubetzka, K. von Bergmann, and R. Wiesendanger, Coexistence of antiferromagnetism and superconductivity in Mn/Nb(110), Phys. Rev. B **105**, L100406 (2022).

[34] K. Park, B. Nyari, A. Laszloffy, L. Szunyogh, and B. Ujfalussy, Effects of strong spin-orbit coupling on Shiba states from magnetic adatoms using first-principles theory, New J. Phys. **25**, 033022 (2023).

[35] T. J. Boerner, S. Deems, T. R. Furlani, S. L. Knuth, and J. Towns, ACCESS: Advancing Innovation: NSF's Advanced Cyberinfrastructure Coordination Ecosystem: Services & Support, in *Practice and Experience in Advanced Research Computing 2023: Computing for the Common Good*, *PEARC '23* (Association for Computing Machinery, New York, 2023), pp. 173–176.